Journal of Pharmaceutical Sciences 000 (2021) 1–10

Contents lists available at ScienceDirect

Journal of Pharmaceutical Sciences

journal homepage: www.jpharmsci.org

Pharmaceutics, Drug Delivery and Pharmaceutical Technology

Machine Learning and Accelerated Stress Approaches to Differentiate Potential Causes of Aggregation in Polyclonal Antibody Formulations During Shipping

Alyssa E. Witeof[a], Austin L. Daniels[a], Laura T. Rea[a], Sanli Movafaghi[a], Katherine Kurtz[a], Madison Davis[a], Raymond W Eveland[b], Christopher P. Calderon[a,c], Theodore W. Randolph[a,*]

[a] Department of Chemical and Biological Engineering, University of Colorado Boulder, Boulder, CO 80309, United States
[b] Sealed Air Corporation, Charlotte, NC 28208, United States
[c] Ursa Analytics, Inc., Denver, Colorado 80212, United States

ARTICLE INFO

Article history:
Received 30 December 2020
Revised 18 February 2021
Accepted 19 February 2021
Available online xxx

Keywords:
Protein aggregation
Machine learning
Protein formulation
Antibodies

ABSTRACT

Therapeutic proteins are among the most widely prescribed medications, with wide distribution and complex supply chains. Shipping exposes protein formulations to stresses that can trigger aggregation, although the exact mechanism(s) responsible for aggregation are unknown. To better understand how shipping causes aggregation, we compared populations of aggregates that were formed in a polyclonal antibody formulation during live shipping studies to populations observed in accelerated stability studies designed to mimic both the sporadic high g-force and continuous low g-force stresses encountered during shipping. Additionally, we compared the effects on aggregation levels generated in two types of secondary packaging, one of which was designed to mitigate the effects of large g-force stresses. Aggregation was quantified using fluorescence intensity of 4,4′-dianilino-1,1′-binaphthyl-5,5′-disulfonic acid (bis-ANS) dye, size exclusion high performance liquid chromatography (SEC—HPLC), and flow imaging microscopy (FIM). FIM was also combined with machine learning methods to analyze particle morphology distributions. These comparisons revealed that the morphology distributions of aggregates formed during live shipping resemble distributions that result from low g-force events, but not those observed following high g-force events, suggesting that low g-force stresses play a predominant role in shipping-induced aggregation.

Introduction

Therapeutic proteins offer many advantages (e.g. potency, mechanism)[1–3] over conventional pharmaceuticals, and comprise the fastest growing class of new drugs.[1,2] Because the safety and efficacy of protein therapeutics depends on their conformation and higher-order structure, it is critical that they are processed and formulated to minimize physical instabilities such as aggregation. Protein aggregation and the associated formation of subvisible particles within formulations can result from a variety of stresses incurred during manufacturing, fill-finish processing, shipping, or administration to patients.[4–11]

A number of mechanisms may be responsible for protein aggregation. The pathways leading to protein aggregation depend on the type of applied stress (e.g., mechanical, thermal, chemical), and result in particles with characteristic morphology distributions. These distinct morphology distributions provide "fingerprints" that may be used to identify the types of stress that generated populations of aggregates within a formulation.[12–14]

We have recently demonstrated a technique that utilizes flow imaging microscopy (FIM) and various machine learning and statistical tools to compare samples based on these particle morphology distributions.[12] FIM uses a digital microscope to record images of particles present in liquid formulations as samples are pumped through a microfluidic channel. The resulting images, while primarily used to count and size particles in a sample, also capture morphological features of the protein aggregates in the sample. This morphology information can be extracted and compared between samples to determine if those samples exhibit similar particle morphology distributions suggesting that the aggregates were formed by a shared aggregation mechanism.

Although great strides have been made in controlling aggregation during manufacturing and fill-finish operations, shipping still

* Corresponding author.
E-mail address: theodore.randolph@Colorado.EDU (T.W. Randolph).

https://doi.org/10.1016/j.xphs.2021.02.029
0022-3549/

exposes protein formulations to potentially damaging thermal and mechanical stresses.[8] Previous studies have evaluated the effects of high g-forces incurred during shipping and have explored potential mitigation of aggregation through improved packaging.[15,16] Other studies have addressed the role of fill volume on protein aggregation in solutions subjected to mechanical stresses.[8] However, our understanding of the relative importance of the various stresses imposed on protein formulations during shipping and ways in which these stresses can be mitigated are still incomplete. For instance, during transportation, protein solutions are typically subjected to low g-force mechanical stresses that may include slow rocking motions and nearly continuous low-intensity vibrations, and sporadic, high g-force mechanical shocks that may induce cavitation. But it is unknown which of these types of motion might be most damaging. In principle, if the stress that predominately causes protein aggregation during shipping could be identified, packaging or shipping conditions could be tailored to specifically address the most damaging stress.

In this study of shipping-induced protein aggregation, intravenous immunoglobulin (IVIg) formulations were filled in glass vials to various fill volumes and packaged in one of two types of secondary packaging designed to modulate the effects of mechanical stresses on the samples. These samples were then exposed to either live shipping stress or one of two accelerated stability stresses designed to mimic the effects of either continuous low g-force motions or sporadic, high g-force mechanical shocks encountered during shipping. A g-force tracking monitor was used to monitor the strength of mechanical shocks incurred by the formulations during these stresses. Protein damage from shipping and in-lab simulated shipping was assessed using aggregate-sensitive extrinsic fluorescence assays, size exclusion high performance liquid chromatography (SEC—HPLC) and FIM.[17] Finally, convolutional neural network (ConvNet)-based machine learning algorithms were used to compare the morphology distributions of aggregates formed in IVIg formulations exposed to real-time shipping stresses to morphology distributions of aggregates formed during accelerated mechanical stresses. The ConvNet algorithm enabled us to discern whether the aggregate populations formed during shipping exhibited morphologies similar to those created by application of low or high g-force shocks. This analysis allowed us to probe the relative importance of these stresses imposed on IVIg formulations during shipping and the contributions of packaging materials to protect samples from shipping-induced damage.

Materials and methods

Materials

A working solution of 0.5 mg/mL intravenous immunoglobulin (IVIg) was prepared by diluting 100 mg/mL Gammagard Liquid (Baxter, Deerfield, IL) in 1x phosphate buffered saline pH 7.4 (Gibco, Carlsbad, California). Nominal 5 mL Type 1 borosilicate glass vials (DWK Life Sciences, Milville, NJ) and butyl rubber stoppers (Fisher, Waltham, MA) were triple washed with filtered 200 proof ethanol (Decon Labs, King of Prussia, PA), tripled rinsed with ultrapure (18.2 MΩ filtered) water, and allowed to air dry before use. 4,4′-dianilino-1,1′-binaphthyl-5,5′-disulfonic acid (bis-ANS), sodium sulfate, sodium phosphate monobasic, and sodium azide were purchased from Sigma Aldrich (St. Louis, MO). Sodium phosphate dibasic was purchased from Fisher Scientific (Waltham, MA).

Sample preparation

IVIg solutions were filled in vials to eight different fill levels, with volumes ranging from 2 to 8.74 mL. The interfacial area-to-volume (IAV) ratio, defined as the ratio of the air-liquid interface area to the liquid volume in the vials, was estimated for each fill volume by modeling the vials as partially filled horizontal cylinders. The total air-water interfacial area was calculated as the sum of the air-liquid surface area and the air-glass surface area above the meniscus which is wetted during agitation and thus contributes additional air-liquid interface area. The surface area in the neck of the vial was not included in the calculation for simplicity's sake. The total air-water interfacial area of the vial was then divided by the liquid fill volume to calculate the IAV ratio, which decreased from 11 to 1.3 cm^{-1} as the fill volume was increased from 2 to 8.7 mL.

Vials were packed in one of two kinds of packaging materials. In packaging denoted as “lab packaging” (LAP), vials were wrapped with bubble wrap and placed in plastic boxes. Another set of vials were packaged in a custom rigid foam packaging from Sealed Air Corporation (Charlotte, NC) designated as “SAP”. SAP packaging was designed to attenuate high frequency, high g-force shocks.

Shipping study

IVIg solutions in vials were packaged in LAP and SAP and were placed in a cardboard overpack with ice packs to maintain temperature and shipped together. Vials were shipped from Colorado to North Carolina via Carrier 1 and returned via Carrier 2. After the return shipping, vials were stored at 4 °C prior to analysis.

Accelerated simulated shipping studies

Accelerated simulated shipping studies were developed to mimic two of the types of stress experienced during shipping: sporadic high g-force events and repetitive low g-force events. To simulate high g-force events that occurred during shipping, IVIg solutions in vials packaged with LAP or SAP (Supplementary Figure S1) were tumbled in a rotary high repetition drop instrument (Roper, Benton Harbor, MI). The instrument dropped the packages from a height of approximately 18 inches once every second. Packages were tumbled for 5, 10, or 15 min at room temperature.

To mimic repetitive low g-force events occurring during shipping, IVIg solutions in vials packaged with LAP or SAP vials were placed on an orbital shaker with a speed of 320 rpm for 0.5, 1, 2, or 4 h at room temperature. Vials were placed within their packaging so as to maintain a horizontal orientation.

Evaluation of g-forces in simulated and live shipping studies

A Shocklog 298 (ShockWatch, Inc., Dallas, TX) impact recorder was included in the shipped package to monitor the g-forces experienced during live shipping. The Shocklog was placed in the overpack to monitor the g forces experienced by both the SAP and LAP samples. The Shocklog continually monitored g-forces and the temperature of the package, recording the maximum g force value experienced by the package over a minute-long interval. The device was set with a maximum threshold of 100 x g (instrument accuracy ± 2%). The Shocklog 298 was also packaged in SAP and LAP and placed in the rotary high repetition drop instrument and on the orbital shaker to characterize the forces experienced by the samples during accelerated simulated shipping stresses.

Extrinsic fluorescence analysis of protein aggregation

4,4′-dianilino-1,1′-binaphthyl-5,5′-disulfonic acid (bis-ANS), an aggregate-sensitive fluorescent dye, was used to assess protein aggregation generated during simulated in-lab shipping and live shipping stresses. Immediately prior to analysis, 20 μL of 25 μM bis-ANS was mixed with 180 μL of sample in a 96-well fluorescence plate (Greiner Bio-One, Kremsmünster, Upper Austria) as previously

described.[18] Plates were read using a microplate reader (Tecan, Mannedorf, Switzerland) with an excitation wavelength of 390 nm and an emission wavelength of 490 nm.

Size exclusion high performance liquid chromatography (SEC—HPLC)

SEC—HPLC was used to determine the amount of soluble protein lost as aggregates during live and accelerated shipping stresses. To prepare samples for SEC—HPLC, 1 mL of each IVIg sample was centrifuged at 20,000 x g for 20 min at 20 °C to sediment insoluble aggregates. 100 μL of the supernatant was injected into an Agilent 1100 HPLC system. The mobile phase consisted of 100 mM sodium sulfate, 50 mM sodium phosphate dibasic, 50 mM sodium phosphate monobasic, and 0.05% sodium azide. Mobile phase flowed through TSKgel Guard SWXL and TSKgel G3000 SWXL analytical columns (Tosoh Bioscience, King of Prussia, PA) at a rate of 0.6 mL/min. Protein concentrations in the eluates were monitored by absorption measured at 280 nm. All chromatograms showed a large peak assigned to monomeric protein that eluted at 15 min, and a smaller peak assigned to soluble minor high molecular weight (HMW) species that eluted at approximately 13 min and comprised roughly 6.3% of the total chromatogram area (see Supplemental Figure S2). The height of the HMW peak was essentially invariant under all conditions tested, even when substantial amounts of aggregate could be observed visually in the samples. Chromatograms were integrated to provide the total peak area for the total soluble protein (i.e., monomer plus HMW) species and compared against chromatograms measured for unstressed controls to determine the amounts of protein lost as insoluble aggregates.

Flow imaging microscopy analysis of particle morphology and concentration

FIM was used to record concentrations and morphology information for particles in samples following application of simulated and live shipping stresses. Samples were analyzed using a FlowCam VS (Fluid Imaging, Scarborough, ME) fitted with a FC80 flow cell and a 10x objective. 150 μL of each sample was loaded into the instrument, of which 100 μL was analyzed at a flow rate of 0.05 mL/min. RGB color images of particles larger than 2 μm in diameter were recorded and analyzed.

Particle comparison algorithm

FIM images of particles produced in IVIg solutions during shipping and accelerated stress testing were analyzed with an image analysis algorithm described previously.[12] This approach uses ConvNets to compress FIM images into very low-dimensional image representations or embeddings and statistical tools such as nonparametric density estimates and goodness-of-fit hypothesis testing to determine if two samples exhibit similar populations of these image embeddings. We briefly describe the application of this algorithm here, noting that the omitted details match those used in a previous study.[12]

FIM images of particles were imported into Python 2.7 and rescaled to 24 × 24 pixels. A ConvNet was trained on FIM images of IVIg aggregates formed in both LAP and SAP as a result of the two accelerated simulated shipping stresses (5 min of tumbling or 0.5 h of shaking) in vials with an IAV ratio of 1.3 cm^{-1} . This network was trained using a triplet loss approach[19] implemented in Keras using a TensorFlow backend. The trained network was used to map FIM images onto 2D image representations or embeddings to capture particle information recorded in the raw images. 9000 FIM images of aggregates generated by each combination of accelerated shipping stress and packaging were used to train this network. 10,000 FIM images from all samples were used as test data for the trained algorithm —including samples stressed during the live shipping study and or stressed at different IAV ratios that were not used to train the initial ConvNet. The resulting point clouds of 2D embeddings were used to compare particles formed by different stresses (real-time shipping or the accelerated shipping stresses) in the same packaging or different packaging when exposed to the same stress. These comparisons were performed both by visual inspection of the embeddings from these conditions as well goodness-of-fit hypothesis testing. To perform hypothesis testing, the ConvNet was used to compute embeddings of all training images recorded under one of the conditions being compared, which we denote as the baseline condition. The resulting embeddings were then used to construct a kernel density estimate of the probability density function (PDF) of embeddings for the baseline condition. Sets of 20 test images were then subsampled from the images recorded under another condition (denoted as the test condition), converted to 2D embeddings using the trained ConvNet and analyzed using a goodness-of-fit hypothesis test to test the null hypothesis that these embedding sets were consistent with the embedding PDF for the baseline sample. This analysis was performed using a Rosenblatt transform-based goodness-of-fit hypothesis test[12] using a 5% Type I (false positive) error rate to determine critical values for the test. This process was repeated 10,000 times per pair of baseline and test samples and the rejection rate (i.e., the fraction of these subsamples that were not consistent with the baseline condition) was recorded as a measure of dissimilarity between the conditions. Samples with very similar particle morphology population distributions yielded rejection rates close to the 5% Type I error rate of the test, whereas samples with more significant differences in particle populations yielded higher rejection rates.

Results

G-forces generated during shipping and accelerated lab testing

The g-forces monitor recorded the average maximum g-force experienced every minute during shipment. A wide range of g-forces were recorded during shipping (Fig. 1A). During Leg 1, Colorado to North Carolina via Carrier 1, numerous short bursts of high g-force events (>30 g) interspersed between longer periods with lower g-forces were observed. During Leg 2 fewer high g events but more shocks in the 1–5 g range were recorded. The temperature recorded by the Shocklog 298 monitor within the shipping box during this leg dropped below freezing for approximately 18 h. It is unclear whether the contents of the vials - which had been packaged within SAP or LAP secondary packaging and arrived unfrozen - experienced a freeze-thaw event during this interval.

Fig. 1B shows the g-forces recorded in the accelerated stress studies when the Shocklog 298 was packed in LAP and SAP and subjected to tumbling and shaking . High g-forces (ca. 30 g) were recorded at ~1-second intervals as the packages dropped repeatedly in the rotary high repetition drop instrument. The g-forces recorded during tumbling in SAP packaging appear to be somewhat attenuated compared to those observed when LAP packaging was used. During shaking, the Shocklog 298 instrument recorded impacts that were characterized by lower g-forces that occurred at a higher frequency than those seen in the tumbling experiments. In contrast to results obtained during tumbling, the packaging type (LAP vs. SAP) had no discernable effect on the magnitude of the g-forces measured in shaking studies.

Fluorescence intensity as function of protein aggregation

Bis-ANS, an extrinsic fluorescence dye, was used to detect aggregates formed in both the lab-simulated and live shipping studies. Fig. 2 shows the effect of stresses (shipping, shaking, and tumbling),

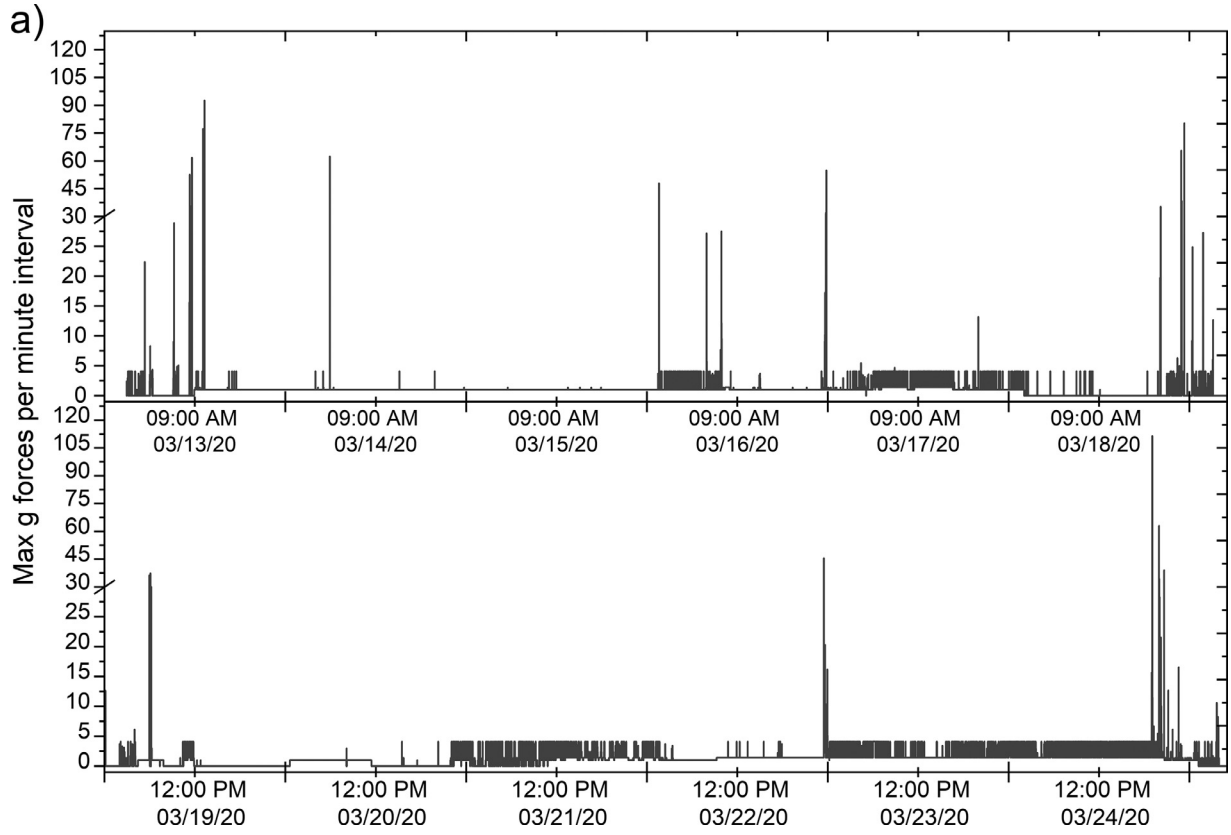

Fig. 1. Shocklog data collected from live shipping study and in-lab accelerated stress studies. A. Root mean square of the max g-forces per minute samples experienced during leg 1 (CO to NC), top, and during leg 2 (NC to CO), bottom. B. Root mean square of g-forces experienced by samples in SAP or LAP from shaking or tumbling stress.

packaging type, and IAV ratio on IVIg aggregation as reflected in fluorescence intensity. Increased fluorescence, and therefore aggregation, was observed as the IAV ratio increased. Fluorescence was increased in samples after shipping, although even greater fluorescence increases were observed in the accelerated studies in spite of their relatively short duration. The packaging type influenced the magnitude of the fluorescence increase observed following application of some stresses. Specifically, SAP appeared to provide more protection (i.e. lower fluorescence intensities corresponding to less aggregation) than LAP against tumbling stress but offered somewhat less protection than LAP against shaking stress.

SEC—HPLC analysis of monomeric protein remaining after shipping and accelerated stress experiments

Samples of IVIg formulations that had been subjected to cross-country shipping, accelerated tumbling stress, or accelerated shaking stress were analyzed via SEC—HPLC to quantify losses of soluble protein. As shown in Fig. 3, all stresses resulted in extensive loss of monomeric protein. Shipped samples that initially contained 0.5 mg/mL IVIg lost between 0.02 mg/mL and 0.14 mg/mL monomeric protein. This loss of monomeric protein increased as the IAV ratio increased. The rate of monomeric protein loss was greatest for samples that were tumbled; application of tumbling stress for only 15 min caused greater protein losses than those incurred in samples shipped round-trip cross-country. Samples with high IAV ratios (corresponding to low fill volumes) that had been packed in SAP packaging showed less fractional protein loss than corresponding samples that had been packed in LAP. Protein losses in samples subjected to shaking for 4 h were larger than those recorded after 15 min of tumbling or after cross-country shipping. There were minimal differences between the protein losses for samples in LAP and SAP following application of shaking stress.

Severe aggregation occurred at later time points in the accelerated stress studies, as was apparent from visually observable cloudiness in the IVIg solutions. While formal appearance testing was not performed for this study, when handling these protein solutions, small globules of aggregated protein were observed to adhere to pipette tips. This stickiness may have led to falsely decreased fluorescence intensity measurements and flow imaging counts. In contrast, because the HPLC analysis measured remaining soluble protein levels rather than the aggregates and particles themselves, it likely provided a more accurate quantification method.

Flow Imaging Microscopy (FIM) analysis of particle morphology and concentration

FIM analysis was performed on all samples to characterize changes in the number and morphology of subvisible (i.e. of size >2 μm in diameter) protein aggregates in each sample. As shown in Fig. 4, particle counts in shipped samples increased with increasing IAV ratio. After round-trip shipping, concentrations of particles in size ranges 10–25 μm and > 25 μm exceeded USP ⟨788⟩ limits for particles in products for parenteral administration[20] (Table 1). In general, formulations shipped in vials that had been packaged in the SAP packaging had fewer particles than those packaged in LAP.

In accelerated studies, the increase in particle counts was more pronounced with both tumbling stress and shaking stress for samples packaged in LAP (Fig. 4). Consistent with the results from shipping studies, lower particle counts were observed in samples with lower IAV ratios exposed to either accelerated shaking or tumbling stresses. Shaking generally produced larger particles than did tumbling, and

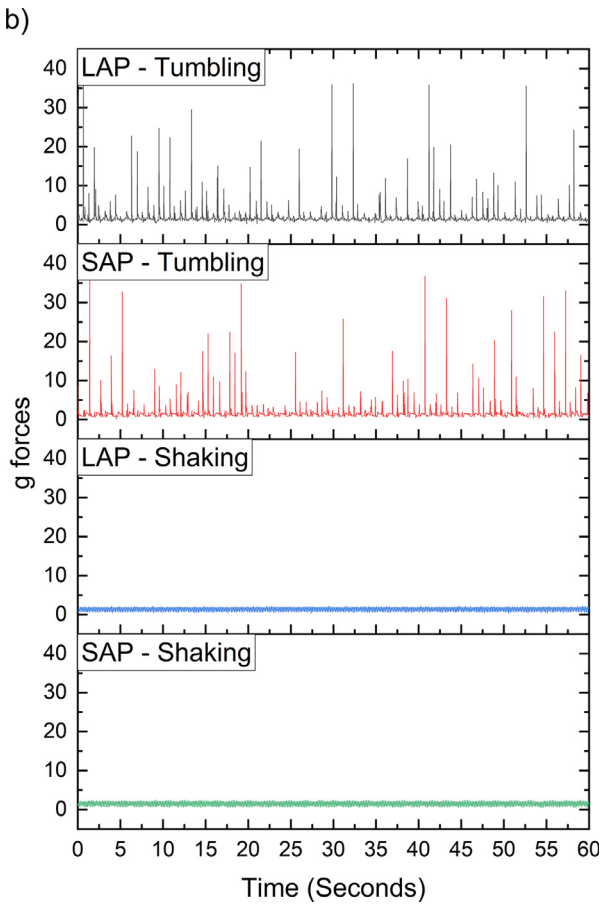

Fig. 1. Continued.

fewer particles >25 μm in size were observed when vials were packaged in SAP packaging (Table 1). After shaking for longer periods of time, the total number of particles detected by FIM plateaued or even decreased. This phenomenon is likely explained by the agitation-dependent agglomeration of many smaller particles to form fewer, larger particles Consistent with this interpretation, higher numbers of large particles >10 μm and increasing levels of fluorescence intensity were observed in samples where the total FIM counts plateaued or were decreasing.

The collections of particle images recorded using FIM (Fig. 5) after samples were subjected to tumbling or shaking stress appeared to be visually different. A small subset of particles in tumbled samples were dark in color and roughly spherical, qualitatively resembling air bubbles with small protein aggregates attached to the outside of the bubbles. In contrast, particles in shaken samples were typically lighter in color and frequently consisted of multiple small particles stuck together. Machine learning approaches were applied to further analyze these observed differences in particle morphology.

Particle comparison algorithm

Raw FIM images were converted using a ConvNet to 2D embeddings that best captured the particle information in the full image. Fig. 5 shows the estimated population density of image embeddings obtained from aggregates generated in vials filled to a 1.3 cm^{-1} IAV ratio by shaking, tumbling, and shipping stresses when packaged in either LAP or SAP. The embedding space learned by the network appears to divide FIM image embeddings into two main clusters on the left and right side of the embedding space. These groups delineate particles formed by shaking and tumbling stress: aggregates formed by shaking generally embed in the right cluster while those formed by tumbling generally embed in the left cluster. Fig. 6 also shows sample FIM images from each stress condition that maps to specific regions of the embedding space. FIM images that embed in the left cluster typically exhibit dark, circular morphologies while those that embed in the right cluster exhibit lighter, more amorphous morphologies. Interestingly, FIM images that were mapped to the same region of the embedding space in Fig. 6 exhibit visually similar particle morphology. While it is important to note that the image features used to compute image embeddings are not always readily human interpretable,[12,21] the visual consistency between FIM images that are mapped to a single region of the embedding space suggests that these embeddings may be related to visually observable particle morphology features.

The ConvNet trained in this analysis was able to easily differentiate particle morphologies generated by shaking from those arising from application of tumbling stress, but was less effective at differentiating particle morphologies in vials packaged in LAP compared to those packaged in SAP. Particle morphology distributions produced by tumbling were more impacted by packaging than those produced by shaking. Particles formed by tumbling vials in SAP instead of LAP packaging exhibited increased embedding density near the leftmost mode of the PDF, suggesting different mechanisms of aggregation between the two packaging types. In contrast, particles produced by shaking vials packaged in SAP exhibited embeddings relatively similar to those of particles made in LAP packaging and were thus likely formed by similar mechanisms. These results were confirmed using goodness-of-fit hypothesis testing. Sets of 20 randomly selected image of particles produced under shaking stress in SAP packaging were differentiable from those produced in LAP packaging 21% of the time, but 67% of the time when particles were produced under tumbling stress. While particles formed by both stresses were impacted by the packaging, the higher rejection rate for particles made by tumbling suggests a stronger packaging effect for that stress overall.

As shown in Fig. 6, the embedding maps of particles produced by shipping stresses in both types of packing materials closely resembled those particle populations generated in accelerated shaking stress studies. Aggregates formed by shipping stress also exhibited visually similar morphologies to those generated by shaking stress (Fig. 6, collages). While the results in Fig. 6 were recorded at a constant IAV ratio (1.3 cm^{-1}), the embedding maps for particle produced during shipping were independent of the vial fill volumes (Fig. 7), suggesting that the dominant mechanisms of particle formation were not dependent on the IAV ratio. Neither fill volume nor packaging material visually appeared to influence the particle populations formed via agitation. This result was confirmed using goodness-of-fit hypothesis testing. Randomly selected sets containing 20 FIM images of particles recorded in sample packaged in SAP could not be distinguished from those produced in LAP using the same fill volume at rates higher than 5%, the Type I error rate of the test. Similarly, the goodness-of-fit hypothesis test failed to distinguish particles produced at different IAV ratios from those produced at an IAV ratio of 1.3 cm^{-1}.

Discussion

The formation of protein aggregates may not only reduce efficacy of therapeutic proteins, but may also provoke adverse immune responses. For example, in vitro studies of IVIg aggregates conducted in human serum show that these aggregates may induce complement activation[11,22] which is associated with adverse events such as anaphylactic shock, altered antibody responses, and impaired immune response.[23,24] Thus, the presence of aggregates in all of our shipped samples at levels that surpassed USP ⟨788⟩ guidelines is concerning.

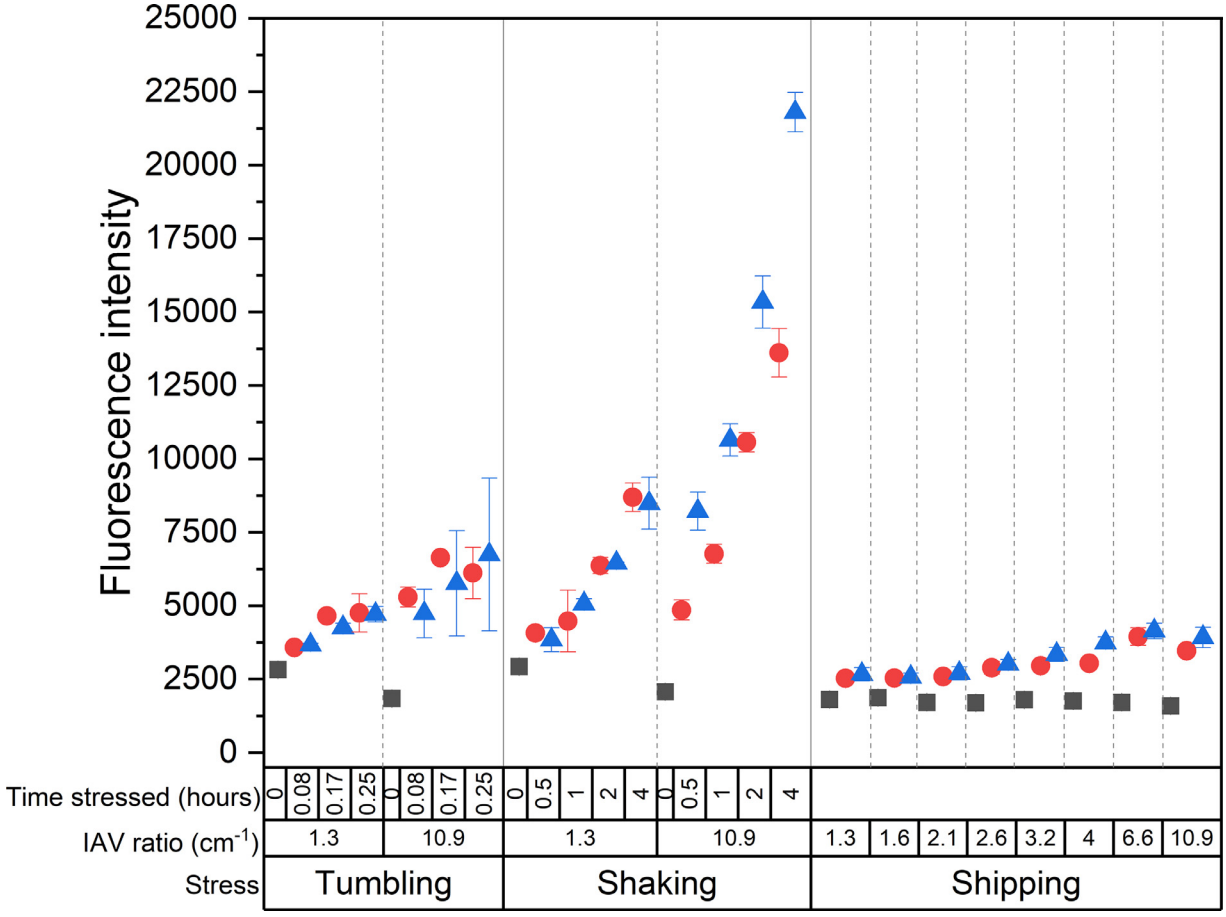

Fig. 2. Bis-ANS fluorescence intensity by time and IAV ratio after tumbling, shaking, or shipping in SAP or LAP. Symbols represent samples from vials packaged in LAP (red circles), SAP (blue triangles), and references (black squares). Data presented as the mean ± standard deviation. Tumbling and shaking studies had an $n = 3$ for each condition and shipping had an $n = 4$ for each condition.

Identifying the types of stresses that are most responsible for forming aggregates during a given process can be useful to guide strategies for reducing process-induced aggregation. Analyses of aggregate morphology distributions such as the FIM + ConvNet approach used here allow evaluation of the relative contributions of various stresses incurred during processes like shipping. Aggregates generated by different mechanisms[25] yield distributions of aggregate morphologies that are characteristic of the root cause stress.[12–14,26] Since aggregate morphology distributions are sensitive to the root cause of aggregation, we can use these distributions as "fingerprints" to identify underlying causes of aggregation during a process by comparing the aggregate morphology distributions produced during a process with standard distributions created by applying isolated, individual stresses in accelerated stability studies.

This approach was used to identify the relative contributions of different mechanical stresses to protein aggregates formed during shipping stress. To this end we mimicked individual stresses that protein therapeutics might experience during shipment and not stresses designed to conform to ISTA or ASTM standards. Multiple types of stresses may be present in a given process operation, making it difficult to ascertain which mechanism might be dominant. For example, Gikanga and Maa[27] recently reviewed how a number of factors complicated efforts to determine dominant mechanisms of aggregate formation during mixing operations. Similarly, in the present case, the wide ranges of characteristic frequencies and amplitudes of motions imposed during shipping present different kinds of stress that could potentially cause protein aggregation. Shaking-based accelerated studies applied high frequency, low magnitude g-forces to the IVIg-containing vials, whereas during tumbling, vials were subjected to less frequent, but much larger g-forces (Fig. 1B). In the live shipping studies, the recorded g-forces were characteristic of a blend of both types of accelerated studies (Fig. 1A), prompting us to question which type of motion may be predominately responsible for aggregation during shipping. We anticipated that the occasional high g-force events observed during shipping would have been most closely linked to aggregate formation. High g-force events like those encountered during tumbling or live shipping stress can be extremely damaging to proteins. These large g-force events can lead to cavitation (the formation of a gas bubble within a liquid) events and concomitant high shear events near container-water interfaces.[5–7] As shown in our prior work,[5–7] dropping primary containers on a solid surface can expose the solution inside the container to severe mechanical shock that can induce cavitation. During cavitation events caused by mechanical shock, a bubble forms and collapses in a violent process with release of large amounts of energy, causing the formation of strong liquid jets and high transient temperatures — each of which can denature a protein.[28–30] Furthermore, prior reports[31,32] have shown that upon instantaneous bubble collapse, protein monomers absorbed to the bubble surface can condense to form various types of aggregates.

However, in contrast to our initial anticipation, the ConvNet-generated 2D embeddings of FIM images obtained from shipped samples

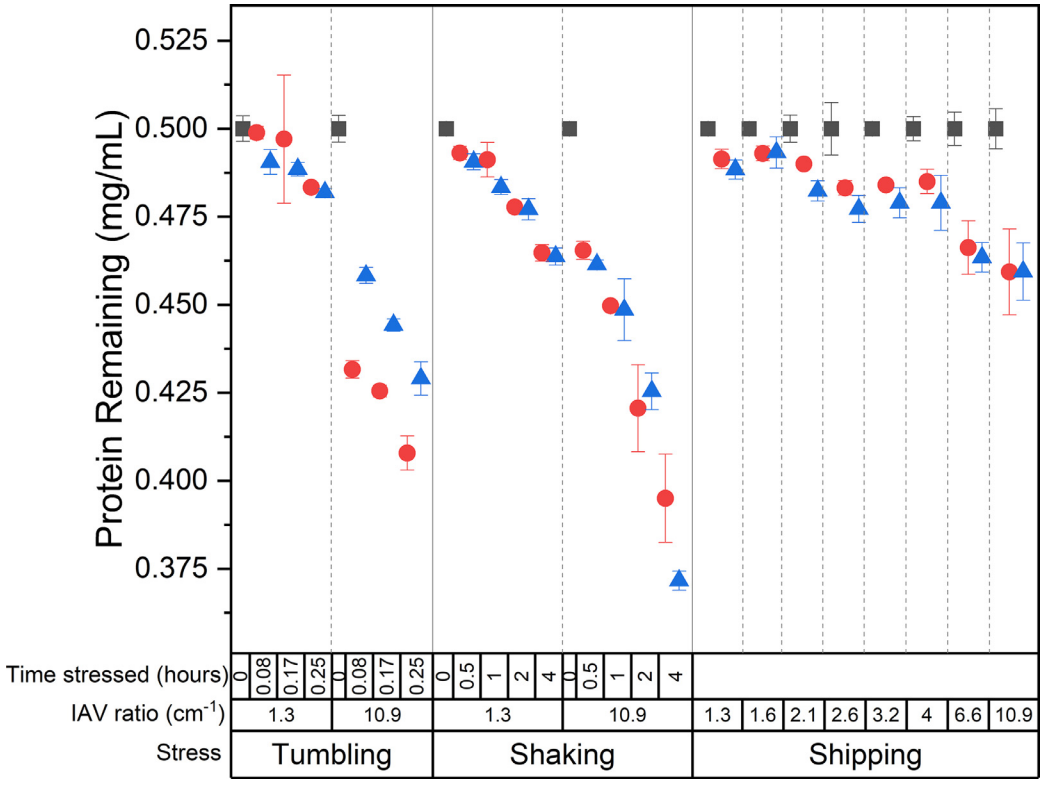

Fig. 3. Soluble protein remaining by time, IAV ratio, and stress type. Soluble protein determined using SEC—HPLC. Symbols represent samples from vials packaged in LAP (red circles), SAP (blue triangles), and references (black squares). Data presented as the mean ± standard deviation. Tumbling and shaking studies had an $n = 3$ for each condition and shipping had an $n = 4$ for each condition.

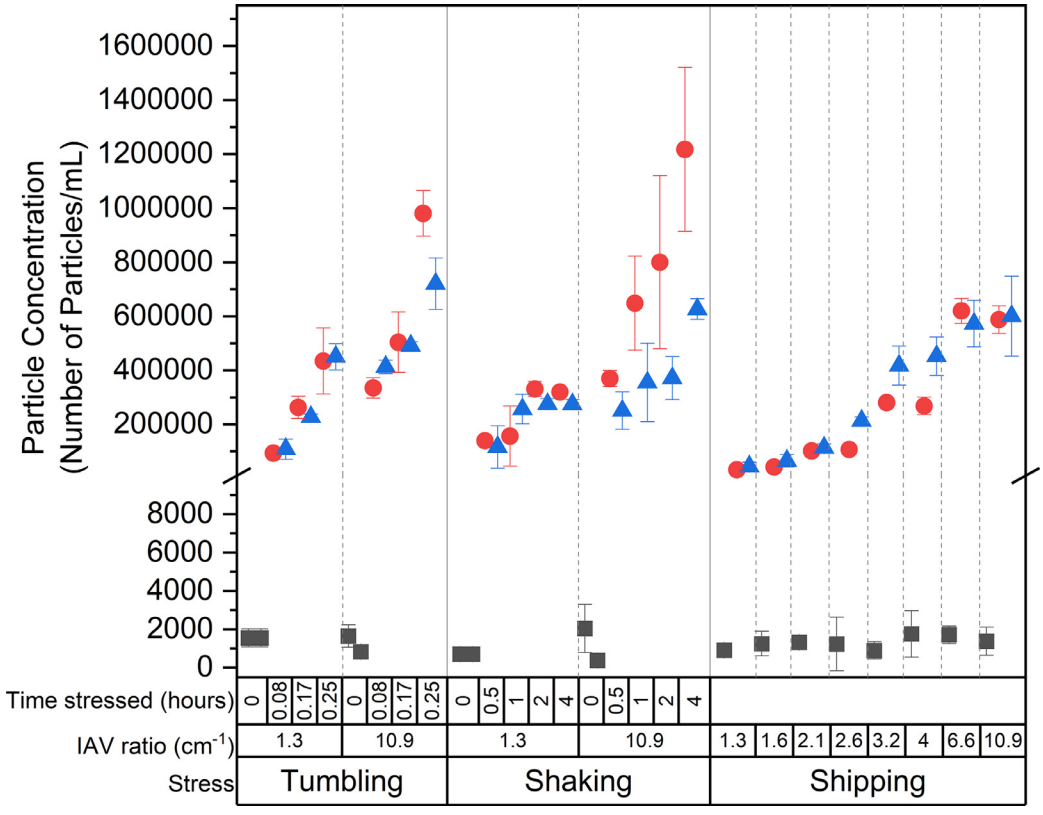

Fig. 4. Particle concentration after tumbling, shaking, or shipping. Concentration of particles by time, IAV ratio, and stress type in SAP or LAP. Symbols represent samples from vials packaged in LAP (red circles), SAP (blue triangles), and references (black squares). Axis break included to better show reference samples. Dashed lines separate IAV ratios and solid lines separate stress type. Data presented as the mean ± standard deviation. Tumbling and shaking studies had an $n = 3$ for each condition and shipping had an $n = 4$ for each condition.

Table 1
Particle counts per mL of IVIg samples that were tumbled, shaken, or shipped in LAP or SAP packaging. Particle counts per mL from FIM broken down into particle size bins of 2–10 μm, 10–25 μm, or >25 μm. Data shown are for vials with an IAV ratio equal to 1.3 cm^{-1} packaged in LAP or SAP that underwent tumbling, shaking, or shipping. Data presented as the mean ± standard deviation.

Packaging	Stress	Time stressed (Hours)	Particle count (Number of particles/mL)		
			2–10 μm	10–25 μm	>25 μm
Reference	Tumbling	0	6.4E+02 ± 2.0E+02	4.9E+01 ± 5.3E+01	2.8E+01 ± 1.3E+01
LAP	Tumbling	0.25	8.3E+05 ± 4.3E+04	1.1E+05 ± 8.2E+03	4.2E+03 ± 4.8E+02
SAP	Tumbling	0.25	4.2E+05 ± 4.5E+04	3.0E+04 ± 3.8E+03	3.5E+02 ± 1.1E+01
Reference	Shaking	0	1.4E+03 ± 5.3E+02	1.5E+02 ± 8.4E+01	1.2E+01 ± 1.0E+01
LAP	Shaking	4	2.1E+05 ± 1.6E+04	9.6E+04 ± 4.7E+03	1.3E+04 ± 1.2E+03
SAP	Shaking	4	1.8E+05 ± 2.4E+04	8.2E+04 ± 2.7E+03	1.4E+04 ± 3.9E+03
Reference	Shipping	N/A	7.3E+02 ± 1.8E+02	8.0E+01 ± 1.0E+01	1.0E+02 ± 6.4E+01
LAP	Shipping	N/A	2.7E+04 ± 4.5E+03	4.6E+03 ± 8.3E+02	3.7E+02 ± 1.5E+02
SAP	Shipping	N/A	3.7E+04 ± 1.3E+04	7.0E+03 ± 2.6E+03	5.7E+02 ± 1.7E+02

were most similar to those obtained from shaken samples which were only exposed to continuous, low g-force motions (Fig. 6). Further, the particle morphologies produced during shipping and accelerated shaking studies were quite distinct from those produced in the high g-force tumbling studies. Thus, it appears that low g-force events characteristic of shaking motions (such as those that might be experienced moving along a conveyer belt at a distribution center or those associated with air transportation) rather than the large, occasional mechanical shocks (e.g., dropping of packages by a courier) dominated aggregation during shipping.

The effects of the two packaging materials on aggregation were consistent with the interpretation that IVIg aggregation was predominately caused by low g force motions associated with shaking. The SAP packaging, which comprises a polymer foam containing very small air pockets designed to dampen high g-force events, attenuated large mechanical shocks produced during tumbling and was effective at reducing IVIg aggregation during these studies. However, packaging the vials in the more advanced SAP packaging resulted in little attenuation of the low but high-frequency g-forces that the vials experienced during shaking, and was ineffective at reducing shaking-induced aggregation. During live shipping, where a mixture of both kinds of motions were recorded, use of the SAP packaging –which presumably attenuated high g-force impacts but not the high frequency, low g-force motions felt by the vials and their IVIg content– did not reduce the loss of soluble protein.

The high frequency, low g-forces observed during shaking and shipping studies cause sloshing of the liquid (i.e., motion of the free liquid interface inside the primary container). The sloshing event occurs as a result of disturbances applied to partially filled liquid containers.[33,34] The motion of the free liquid interface during shaking of a vial partially filled with protein solutions also causes new air–water interfaces to be introduced into the solution resulting in further protein adsorption and denaturation.[35] The sloshing effect becomes more pronounced as the IAV ratio increases when larger headspace is present, resulting in more protein aggregation and particle formation. Our results showed that IVIg aggregation increased in vials with reduced fill volumes that offered higher IAV ratios. Importantly, however, our results indicate that the mechanism of aggregation was unaffected as headspace was varied. Population distributions of particle morphology determined from ConvNet

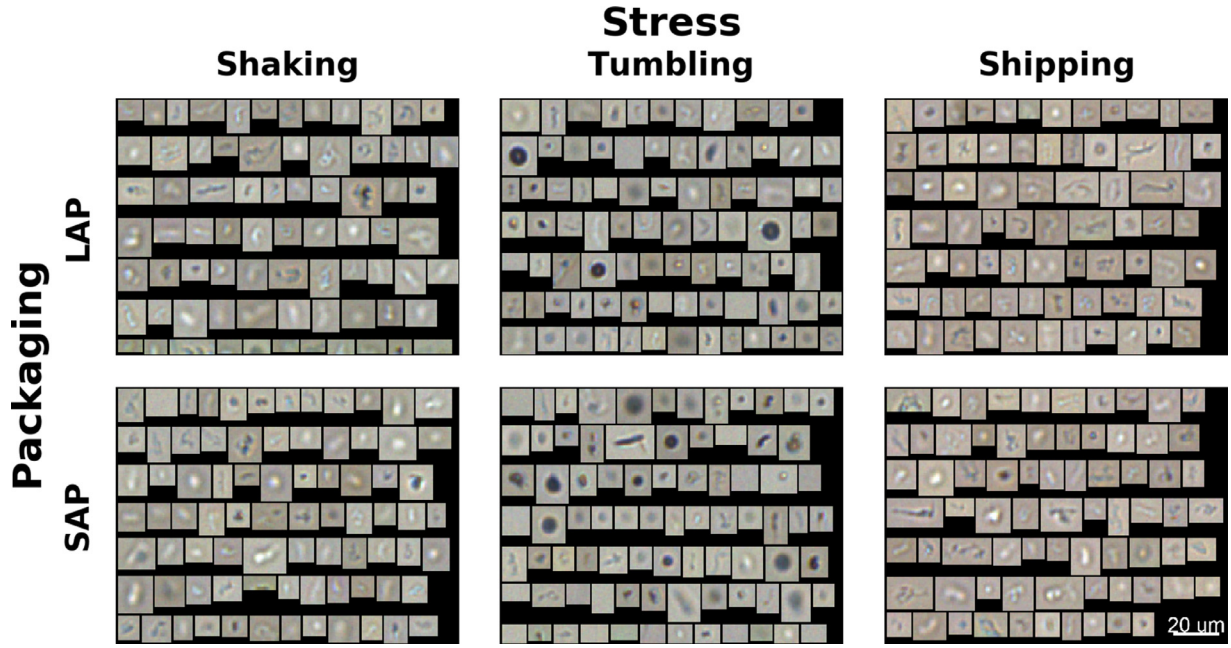

Fig. 5. Randomly selected FIM images of particles from vials packaged in LAP or SAP and filled to a 1.3 cm^{-1} IAV ratio. Particles were formed via shaking, tumbling, or shipping the vials.

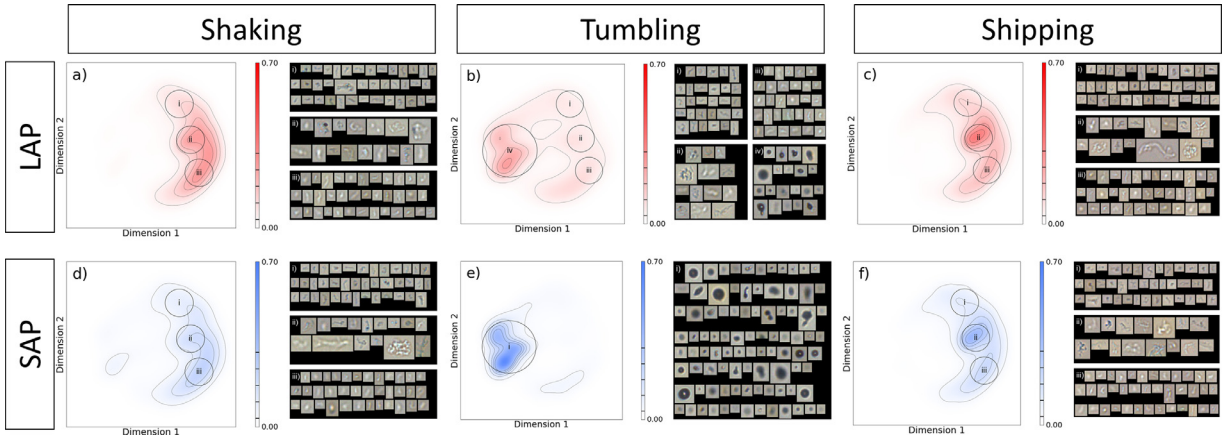

Fig. 6. Contour plots showing the probability density function of ConvNet-derived FIM image embeddings from IVIg aggregates produced in vials filled to a 1.3 cm^{-1} IAV ratio that had been (a) shaken, (b) tumbled, or (c) shipped in LAP as well as those (d) shaken, (e) tumbled, or (f) shipped in SAP. Dimensions 1 and 2 are arbitrary dimensions learned by the trained ConvNet to differentiate the embeddings of aggregates generated by shaking and tumbling as well as those generated in LAP and SAP. The color at a given region of each plot indicates the fraction of FIM image embeddings for that sample located at that region of the embedding space. The density of embeddings at different regions of the figure can be determined using the color bar associated with each figure. Sample FIM images from each image that embedded in the circled regions of the embedding space are shown in the collages to the right of each figure.

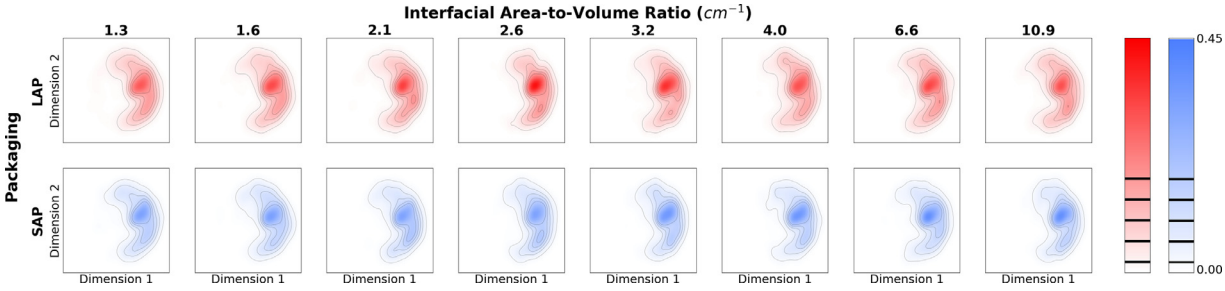

Fig. 7. Contour plots showing the PDF of ConvNet-derived FIM image embeddings from vials with different IAV ratios after shipping in either LAP or SAP. The dimensions and contour plots for each figure are interpreted as described for Fig. 6.

analysis were independent of fill volume (Fig. 7) in spite of the increased amounts of aggregated IVIg observed as IAV ratios increased.

Conclusions

Embedding distributions from ConvNet analyses, here shown to correlate to particle morphology distributions of aggregates produced during cross-country shipping, were similar to those made by shaking but distinct from those created when samples were repeatedly dropped in the rotary high repetition drop instrument, suggesting that stresses imposed by shaking rather than the occasional high g-force events encountered during shipping were the primary drivers of protein aggregation.

The extent, but not the mechanism, of IVIg aggregation correlated with the amount of air-water interfacial area, suggesting that fill-finish strategies that minimize headspaces in vials may be useful in controlling shipping-induced aggregation. Even so, the identification low g force motions as a key type of damaging stress highlights the need for advanced packaging strategies that protect against these stresses during shipping. Use of advanced packaging materials that attenuated high g-force events successfully reduced aggregation caused by multiple dropping events, but this made little difference to shipping-induced aggregation. Our study suggests that most aggregates were formed by shaking type stresses and associated fluid sloshing, a mechanism that is not yet sufficiently addressed by current packaging strategies.

Acknowledgments

The authors would like to thank ShockWatch for their generous donation of a Shocklog 298 and Sealed Air Corporation for providing the SAP packaging and coordinating cross-country shipping of samples.

Funding

This work was supported by Sealed Air Corporation.

Supplementary materials

Supplementary material associated with this article can be found, in the online version, at doi:10.1016/j.xphs.2021.02.029.

References

1. Sauna ZE, Lagassé HAD, Alexaki A, et al. Recent advances in (therapeutic protein) drug development. *F1000Res*. 2017;6.
2. Carter PJ. Introduction to current and future protein therapeutics: a protein engineering perspective. *Exp Cell Res*. 2011;317(9):1261–1269.
3. Pisal DS, Kosloski MP, Balu-Iyer S V. Delivery of therapeutic proteins. *J Pharm Sci*. 2010;99(6):2557–2575.
4. Torisu T, Maruno T, Hamaji Y, Ohkubo T, Uchiyama S. Synergistic effect of cavitation and agitation on protein aggregation. *J Pharm Sci*. 2017;106(2):521–529.
5. Randolph TW, Schiltz E, Sederstrom D, et al. Do not drop: mechanical shock in vials causes cavitation, protein aggregation, and particle formation. *J Pharm Sci*. 2015;104(2):602–611.

6. Movafaghi S, Wu H, Francino Urdániz IM, et al. The effect of container surface passivation on aggregation of intravenous immunoglobulin induced by mechanical shock. *Biotechnol J*. 2020;15(9):1–9.
7. Wu H, Chisholm CF, Puryear M, et al. Container surfaces control initiation of cavitation and resulting particle formation in protein formulations after application of mechanical shock. *J Pharm Sci*. 2020;109(3):1270–1280.
8. Nejadnik MR, Randolph TW, Volkin DB, et al. Postproduction handling and administration of protein pharmaceuticals and potential instability issues. *J Pharm Sci*. 2018;107(8):2013–2019.
9. Randolph TW, Carpenter JF. Engineering challenges of protein formulations. *AIChE J*. 2007;53(8):1902–1907.
10. Wu H, Randolph TW. Aggregation and particle formation during pumping of an antibody formulation are controlled by electrostatic interactions between pump surfaces and protein molecules. *J Pharm Sci*. 2020;109(4):1473–1482.
11. Snell JR, Monticello CR, Her C, et al. DEHP Nanodroplets leached from polyvinyl chloride IV bags promote aggregation of IVIG and activate complement in human serum. *J Pharm Sci*. 2020;109(1):429–442.
12. Daniels AL, Calderon CP, Randolph TW. Machine learning and statistical analyses for extracting and characterizing “fingerprints” of antibody aggregation at container interfaces from flow microscopy images. *Biotechnol Bioeng*. 2020;117(11):3322–3335.
13. Calderon CP, Daniels AL, Randolph TW. Deep convolutional neural network analysis of flow imaging microscopy data to classify subvisible particles in protein formulations. *J Pharm Sci*. 2018;107(4):999–1008.
14. Gambe-Gilbuena A, Shibano Y, Krayukhina E, Torisu T, Uchiyama S. Automatic identification of the stress sources of protein aggregates using flow imaging microscopy images. *J Pharm Sci*. 2020;109(1):614–623.
15. Dill S, Brees K, Stahly A, Cheng E, Carpenter J, Caplan L. Mechanical shock during shipping of medications: the roles of packaging and transportation vendors. *J Pharm Sci*. 2020;109(1):670–676.
16. Siska C, Harber P, Kerwin BA. Shocking data on parcel shipments of protein solutions. *J Pharm Sci*. 2020;109(1):690–695.
17. Singh SK, Afonina N, Awwad M, et al. An industry perspective on the monitoring of subvisible particles as a quality attribute for protein therapeutics. *J Pharm Sci*. 2010;99(8):3302–3321.
18. Wu H, Randolph TW. Rapid quantification of protein particles in high-concentration antibody formulations. *J Pharm Sci*. 2019;108(3):1110–1116.
19. Schroff F, Kalenichenko D, Philbin J. FaceNet: a unified embedding for face recognition and clustering. *Proc IEEE Comput Soc Conf Comput Vis Pattern Recognit*. 2015:815–823.
20. United States Pharmacopeia. *<788>Particulate matter in injections*. 34. 2011. https://www.uspnf.com/sites/default/files/usp_pdf/EN/USPNF/revisionGeneralChapter788.pdf.
21. Wang H, Wu X, Huang Z, Xing EP. High-frequency component helps explain the generalization of convolutional neural networks. *Proc IEEE Comput Soc Conf Comput Vis Pattern Recognit*. 2020:(Remark 1):8681–8691.
22. Chisholm CF, Behnke W, Pokhilchuk Y, Frazer-Abel AA, Randolph TW. Subvisible particles in IVIg formulations activate complement in human serum. *J Pharm Sci*. 2020;109(1):558–565.
23. Baker MP, Reynolds HM, Lumicisi B, Bryson CJ. Immunogenicity of protein therapeutics: the key causes, consequences and challenges. *Self/Nonself - Immune Recognit Signal*. 2010;1(4):314–322.
24. Bonilla FA. Intravenous immunoglobulin: adverse reactions and management. *J Allergy Clin Immunol*. 2008;122(6):1238–1239.
25. Wang W, Roberts CJ. Protein aggregation – mechanisms, detection, and control. *Int J Pharm*. 2018;550(1–2):251–268.
26. Joubert MK, Luo Q, Nashed-Samuel Y, Wypych J, Narhi LO. Classification and characterization of therapeutic antibody aggregates. *J Biol Chem*. 2011;286(28):25118–25133.
27. Gikanga B, Maa YF. A review on mixing-induced protein particle formation: the puzzle of bottom-mounted mixers. *J Pharm Sci*. 2020;109(8):2363–2374.
28. Van Wijngaarden L. Mechanics of collapsing cavitation bubbles. *Ultrason Sonochem*. 2016;29:524–527.
29. Brennen CE. *Cavitation and bubble dynamics*. Cambridge University Press; 2013.
30. Franc J-P, Michel J-M. *Fundamentals of cavitation*. 76. Kluwer Academic Publishers; 2005.
31. Nakajima K, Ogi H, Adachi K, et al. Nucleus factory on cavitation bubble for amyloid β fibril. *Sci Rep*. 2016;6(1):22015.
32. Duerkop M, Berger E, Dürauer A, Jungbauer A. Impact of cavitation, high shear stress and air/liquid interfaces on protein aggregation. *Biotechnol J*. 2018;13:(7)1800062.
33. Ibrahim RA, Pilipchuk VN, Ikeda T. Recent advances in liquid sloshing dynamics. *Appl Mech Rev*. 2001;54(2):133–199.
34. Kiese S, Papppenberger A, Friess W, Mahler HC. Shaken, not stirred: mechanical stress testing of an IgG1 antibody. *J Pharm Sci*. 2008;97(10):4347–4366.
35. Maa YF, Hsu CC. Protein denaturation by combined effect of shear and air-liquid interface. *Biotechnol Bioeng*. 1997;54(6):503–512.